Part II. Discontinuous Galerkin Method Applied to a Single Phase Flow in Porous Media

Béatrice Rivière, [a] Mary F. Wheeler, [a] Krzysztof Banaś [a,b]

[a] *The Center for Subsurface Modeling,*
Texas Institute for Computational and Applied Mathematics,
The University of Texas, Austin TX 78712, U.S.A.
[b] *Section of Applied Mathematics,*
Cracow University of Technology, Warszawska 24, Kraków, Poland.

Discontinuous Galerkin numerical simulations of single phase flow problem are described in this paper. The simulations show the advantages of using discontinuous approximation spaces. *hp* convergence results are obtained for smooth solutions. Unstructured meshes and unsmooth solutions are also considered.
Keywords: discontinuous approximations, discontinuous coefficients, porous media, single phase flow

1. Introduction

The motivation for applying the discontinuous Galerkin procedure for modeling flow in porous media arises from the fact that this algorithm is mass conservative element by element and that higher order approximations which vary locally can by employed. Unlike the locally conservative mixed finite element method no additional functions such as gradients and complicated higher order approximation methods need to be incorporated into the formulation. Also in contrast with many of the locally conservative control volume schemes which are vertex centered, the discontinuous Galerkin method does not require two different grids. Another interesting feature of this method is that an unusual polynomial space can be chosen for quadrilaterals in 2D and hexahedral and prismatic elements in 3D: the complete polynomial space. This space is well suited for triangular and tetrahedral elements but it has been shown that optimal approximation results still hold for other types of elements. Thanks to the discontinuity

inherent to the method, such space is possible, and the number of unknowns is less important than in usual product spaces. The discontinuous Galerkin method considered in this paper was first formulated by Baumann and Oden in [1,3]. The formulation is based on the work done by Wheeler [7] in the late seventies. This paper consists of three sections after the introduction. In §2, we present the model problem and the discontinuous Galerkin method, as well as the error indicators used for adaptive mesh refinement. In §3, numerical simulations are presented. In the last section, we give some conclusions.

2. Model Problem and Scheme

Let Ω be a convex polygonal domain in $\mathbb{R}^n, n = 2$ or 3 and let $\mathcal{E}_h = \{E_1, E_2, \ldots, E_{N_h}\}$ be a nondegenerate quasiuniform subdivision of Ω. In this paper, the two-dimensional elements E_j are quadrilaterals and the three-dimensional elements E_j are prismatic elements. We denote the edges (resp. faces for $n = 3$) of $\mathcal{E}_h$ by $\left\{e_1, e_2, \ldots, e_{P_h}, e_{P_{h+1}}, \ldots, e_{M_h}\right\}$ where $e_k \subset \Omega, 1 \leq k \leq P_h$, and $e_k \subset \partial\Omega$, $P_h + 1 \leq k \leq M_h$. With each edge (or face) e_k, we associate a unit normal vector $\boldsymbol{\nu}_k$. For $k > P_h$, $\boldsymbol{\nu}_k$ is taken to be the unit outward vector normal to $\partial\Omega$. The direction of the vector $\boldsymbol{\nu}_k$ will define the jump and average of a function ϕ on an edge e_k shared by two elements E_i^k and E_j^k.

$$[\phi] = (\phi|_{E_i^k})|_{e_k} - (\phi|_{E_j^k})|_{e_k}, \quad \{\phi\} = \frac{1}{2}(\phi|_{E_i^k})|_{e_k} + \frac{1}{2}(\phi|_{E_j^k})|_{e_k}.$$

We denote by $\mathcal{D}_r(\mathcal{E}_h)$ the finite element subspace that consists of discontinuous piecewise polynomials of degree r on each element. The variable p is commonly used in the *hp* finite element methods, to denote the polynomial degree. Here, in order to avoid confusion with the pressure variable p, the choice of r has been adopted. We denote the complete polynomials the set of polynomials of total degree equal to or less than r. For prismatic elements, we can also choose the tensor product of polynomials of degree r in the z-direction with the set of complete polynomials of total degree r in x and y directions.

The single phase flow is modeled by the following elliptic problem :

$$\begin{aligned} -\nabla \cdot (K \nabla p) &= f \text{ in } \Omega, \\ p &= p_0 \text{ on } \Gamma_D, \\ K \nabla p \cdot \nu_N &= 0 \text{ on } \Gamma_N, \end{aligned}$$

where p denotes the pressure, K is the permeability field of the medium, and Γ_D (resp. Γ_N) denote the Dirichlet (resp. Neumann) part of the boundary of Ω. In general, K can be a full tensor. In what follows, we assume that the medium is isotropic and that $K = \kappa I$, where κ is piecewise constant on each element and I is the identity tensor. The discontinuous Galerkin approximation of the pressure P^{DG} satisfies the formulation

$$\begin{aligned}\sum_{j=1}^{N_h}\int_{E_j} K\nabla P^{DG}\nabla v - \sum_{k=1}^{P_h}\int_{e_k}\{K\nabla P^{DG}\cdot\boldsymbol{\nu}_k\}[v] + \sum_{k=1}^{P_h}\int_{e_k}\{K\nabla v\cdot\boldsymbol{\nu}_k\}[P^{DG}]\\ - \sum_{e_k\in\Gamma_D}\int_{e_k}(K\nabla P^{DG}\cdot\boldsymbol{\nu}_k)v + \sum_{e_k\in\Gamma_D}\int_{e_k}(K\nabla v\cdot\boldsymbol{\nu}_k)P^{DG}\\ = \int_\Omega fv + \sum_{e_k\in\Gamma_D}\int_{e_k}(K\nabla v\cdot\boldsymbol{\nu}_k)p_0, \qquad \forall v \in \mathcal{D}_r(\mathcal{E}_h).\end{aligned}$$

Theoretical (optimal *hp* type) *a priori* error estimates in the energy norm and the L^2 norms have been obtained in Part I of this work [4]. In the numerical experiments, the mesh is adaptively refined based on the computation of error indicators, introduced in [5,6]. We first solve a local discrete problem defined by: Find $\Phi_h \in \mathcal{D}_r(\mathcal{E}_h)$ such that:

$$\begin{aligned}\int_{E_j} K\nabla\Phi_h\nabla v - \int_{\partial E_j}(K\nabla\Phi_h\cdot\boldsymbol{\nu}_{E_j})v + \int_{\partial E_j}(K\nabla v\cdot\boldsymbol{\nu}_{E_j})\Phi_h\\ = R(v), \quad \forall v\in\mathcal{D}_{r+q}(\mathcal{E}_h),\end{aligned}$$

where q is a positive integer and R is the linear functional associated to the error:

$$\begin{aligned}R(v) = \int_\Omega fv + \sum_{e_k\in\Gamma_D}\int_{e_k}(K\nabla v\cdot\boldsymbol{\nu}_k)p_0 - \sum_{j=1}^{N_h}\int_{E_j}K\nabla P^{DG}\nabla v\\ + \sum_{k=1}^{P_h}\int_{e_k}\{K\nabla P^{DG}\cdot\boldsymbol{\nu}_k\}[v] - \sum_{k=1}^{P_h}\int_{e_k}\{K\nabla v\cdot\boldsymbol{\nu}_k\}[P^{DG}]\\ + \sum_{e_k\in\Gamma_D}\int_{e_k}(K\nabla P^{DG}\cdot\boldsymbol{\nu}_k)v - \sum_{e_k\in\Gamma_D}\int_{e_k}(K\nabla v\cdot\boldsymbol{\nu}_k)P^{DG}\end{aligned}$$

We note that $\mathcal{D}_{r+q}(\mathcal{E}_h)$ is a larger (richer) space than $\mathcal{D}_r(\mathcal{E}_h)$ and we will refer to q as the degree of enrichment of the space. The error indicator for the energy norm of the error is denoted by η_1 and defined by

$$\eta_1 = \left(\sum_{j=1}^{N_h}\eta_{1,j}^2\right)^{\frac{1}{2}}, \quad \eta_{1,j}^2 = \int_{Ej}K(\nabla\Phi_h)^2. \tag{2.1}$$

In all our numerical experiments, we locally refine the elements E_j which exhibit large error indicators $\eta_{1,j}$. Therefore, an element E_{j_0} is refined if $\frac{\eta_{1,j_0}}{\max_j \eta_{1,j}} \geq \delta$, where δ is a parameter ranging between 0 and 1.

3. Numerical Experiments

3.1. 3D Problem with a Smooth Solution

The purpose of this example is to check h and p convergence rates of the discontinuous Galerkin method for a pure diffusion problem with smooth solution and to test different sets of shape functions: tensor product polynomials and complete order polynomials. The domain is the box $[0,1] \times [0,1] \times [0,1]$. The coefficient tensor K is the constant identity matrix. The right hand side and Dirichlet boundary conditions are chosen so that

$$u_{ex} = \exp\left(-x^2 - y^2 - z^2\right)$$

is the exact solution. To show the flexibility of the DG formulation, we first consider a non-conforming mesh shown in Fig. 1. On the left-side of the cube, where the mesh is more refined, the approximation is quadratic. On the other side of the cube,the degree of approximation is chosen to be 5. Fig. 2 shows that isosurfaces of the DG solution are smooth and exhibit proper spherical symmetry. One advantage of the DG method is that one can increase the degree of polynomial locally in regions where the mesh can be coarsened. We then investigate the *hp* convergence rates by solving the problem on a sequence of meshes starting with an initial mesh consisting of two prismatic elements. We apply consecutive isotropic refinements of the mesh and change uniformly the degree of approximation r for all elements. Fig. 3 and Fig. 4 present the *hp* convergence in the L2 norm and H1 seminorm versus the total number of degrees of freedom, for prismatic elements with complete order polynomial basis. The convergence rates agree with the theoretical estimates proven in [4]. They are optimal in the energy norm. In Fig. 5, h convergence rates are compared for tensor product and complete polynomial bases. Tensor product bases give slightly better accuracy but use substantially more degrees of freedom (the ratio for the degree of approximation r is $\frac{3(r+1)}{r+3}$).

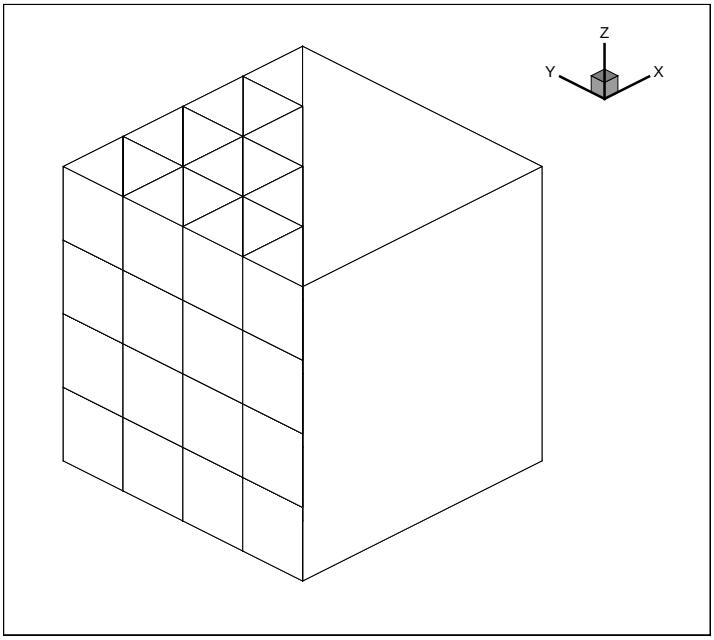

Figure 1. Smooth solution - nonconforming mesh

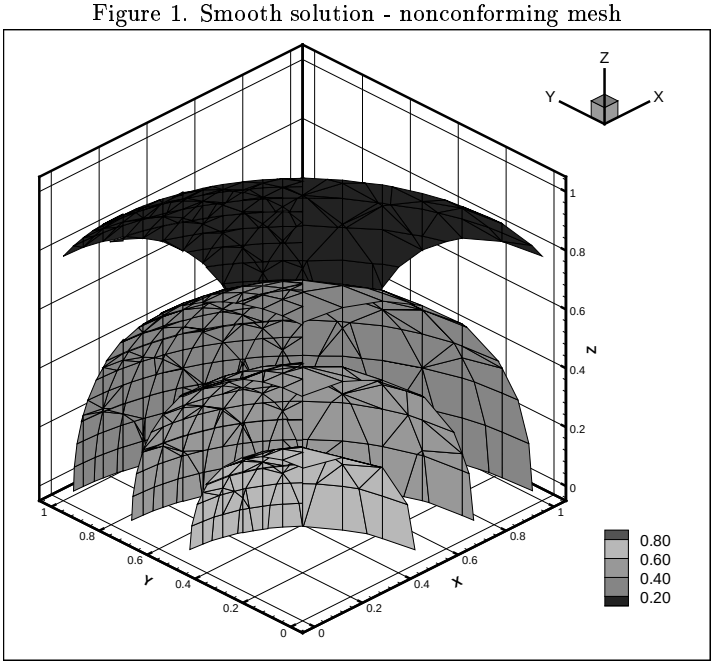

Figure 2. Smooth solution - Isosurfaces of computed solution

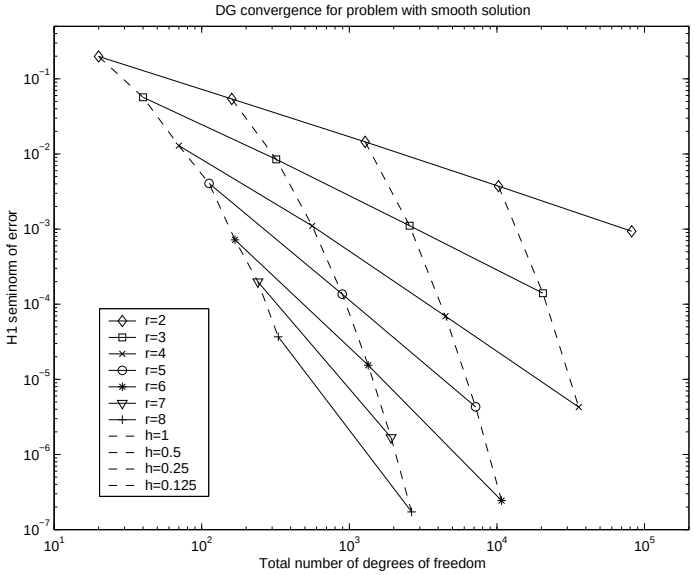

Figure 3. Smooth solution - *hp* convergence rates in H^1 seminorm v. number of degrees of freedom

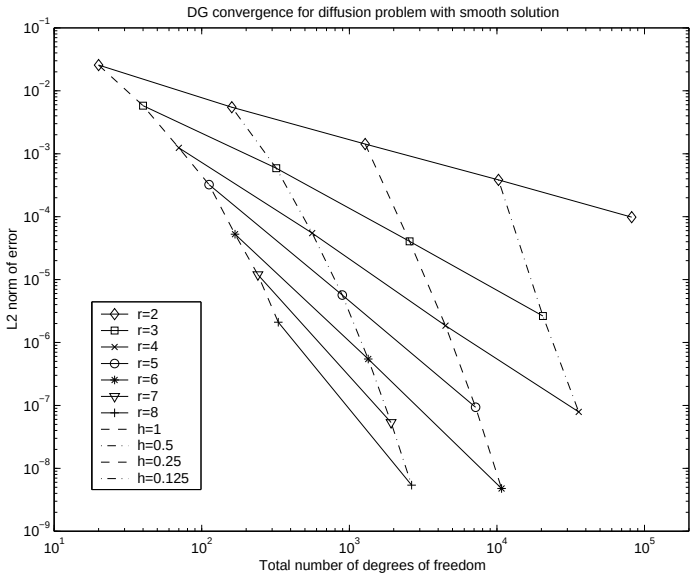

Figure 4. Smooth solution - *hp* Convergence rates in L_2 norm v. number of degrees of freedom

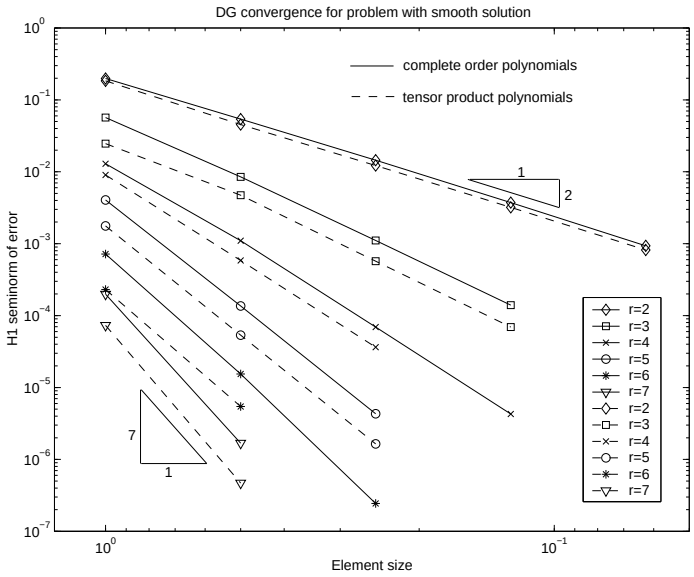

Figure 5. Smooth solution - Convergence rates in H^1 seminorm v. element size h

3.2. Problem with Discontinuous Coefficients

The purpose of this section is to investigate the behavior of the DG method and the effect of the implicit error indicator η_1 described earlier for solutions of elliptic problems with discontinuous coefficients. In real applications, the permeability field may highly vary in space. Here, we consider a simple domain $\Omega = (-1,1)^2$ divided in four sub-domains Ω_i (see Fig.6). The permeability κ takes the constant value κ_i over each sub-domain and we assume that $\kappa_1 = \kappa_3 = 100$ and $\kappa_2 = \kappa_4 = 1$. We seek an analytical solution of the form $r^\alpha(a_i \sin(\alpha\theta) + b_i \cos(\alpha\theta))$, where (r,θ) are the polar coordinates of a given point in Ω and a_i, b_i are constants that depend on the sub-domains Ω_i. The analytical solution p_{ex} satisfies the usual interface conditions: p_{ex} and $\kappa\dfrac{\partial p_{ex}}{\partial n}$ are continuous across the interfaces. It is known that p_{ex} belongs to the Sobolev space $H^\alpha(\Omega)$. Besides, the analytical solution p_{ex} satisfies $-\nabla \cdot K\nabla p = 0$ on Ω. Dirichlet boundary conditions are assumed. In that case, the solution presents a singularity around the origin and we can show that the parameters characterizing the

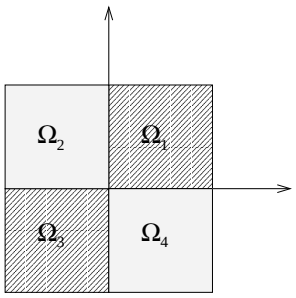

Figure 6. Discontinuous coefficients problem: Initial domain.

analytical solution are the following

$$\begin{aligned}
\alpha &= 0.12690206972221, \\
a_1 &= 0.100000000, \qquad b_1 = 1.000000000, \\
a_2 &= -9.603960396, \qquad b_2 = 2.960396040, \\
a_3 &= -0.4803548672, \quad b_3 = -0.8827565925, \\
a_4 &= 7.701564882, \qquad b_4 = -6.456461752.
\end{aligned}$$

We first analyze the convergence of the DG solution on a sequence of uniformly refined meshes. The coarse mesh consists of the four sub-domains Ω_i. The relative error in the L^2 norm , defined as $\frac{\|p - P^{DG}\|_0}{\|p\|_0}$ is plotted against the number of degrees of freedom in Fig. 7. The degree of the polynomial approximation varies between 2 and 5. We see, as expected, that the convergence rate does not depend on the degree of the approximation, but that it depends on the regularity of the solution. In that case, the convergence rate in the L^2 norm is $O(h^{2\alpha}) = O(h^{0.25})$, where h is the mesh size, or $O(N^{\alpha})$, where N is the number of degrees of freedom. Due to numerical integration errors arising around the origin, one has to compute the H_0^1 norm of the exact solution by using the Green's theorem and by computing a line integral over $\partial\Omega$. In Fig. 8, the convergence of the quantity $A^* = \sum_{j=1}^{N_h} \int_{E_j} K(\nabla P^{DG})^2 - \sum_{j=1}^{N_h} \int_{E_j} K(\nabla p_{ex})^2$ is studied for a degree of polynomial approximation between 2 and 5. It is observed that the rate of convergence is $O(h^{2\alpha})$ or $O(h^N)$, which is the optimal rate usually obtained in the conforming finite element method. As above, the rate of convergence does not depend on the degree of polynomial approximation.

We now investigate the robustness of the adaptation strategy. We begin with a uniform mesh of size $h = 1$ and we adaptively refine the mesh with $\delta = 0.50$

using the strategy described in §2. We fix $r = 2$ and $q = 5$. We investigate the efficiency of the error indicator. For that, we consider the final mesh obtained with the adaptive refinement strategy for $q = 5$. Given a box of size H centered around the origin, we count the number of elements contained in the box. From Fig. 9, one observes that the indicator efficiently captures the singularity of the exact solution around the origin since 72% of the elements are contained in the box of size $H = 0.1$, which corresponds to a subdomain of size $\frac{1}{400}$ of the entire domain. We show in Fig. 10 the final mesh and solution. We see that the mesh is appropriately refined around the origin. Fig. 11 show the error indicators computed on each element. The error indicators are larger in the neighborhood of the origin, which means that the implicit error indicator capture very well the location of the singularity of the exact solution. Fig. 12 and 13 show a close-up view of the computed solution and the local error indicators at the origin. Here, we see that the error indicators possess the same symmetry properties than the exact solution. In Fig. 14, the mesh adaptation strategy yields an optimal convergence rate that is not reached in the case of uniform mesh refinements.

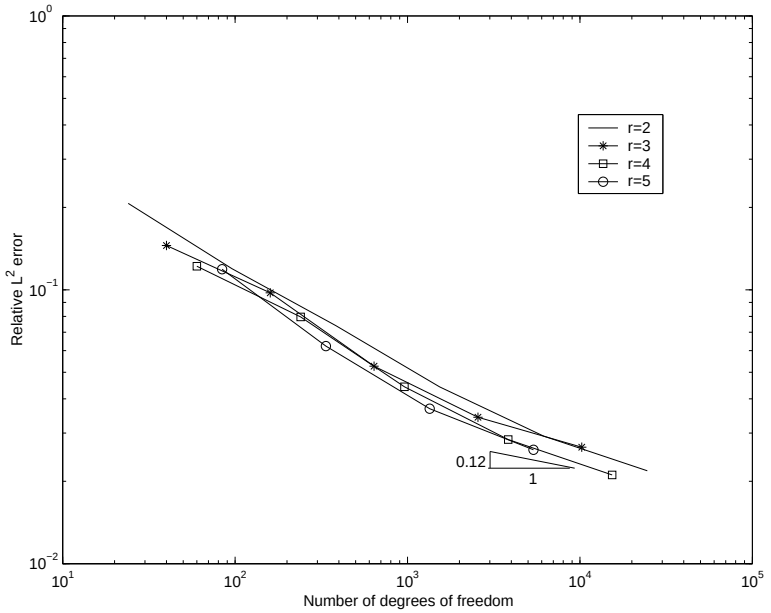

Figure 7. Discontinuous coefficients solution. Relative error in the L^2 norm v. number of degrees of freedom.

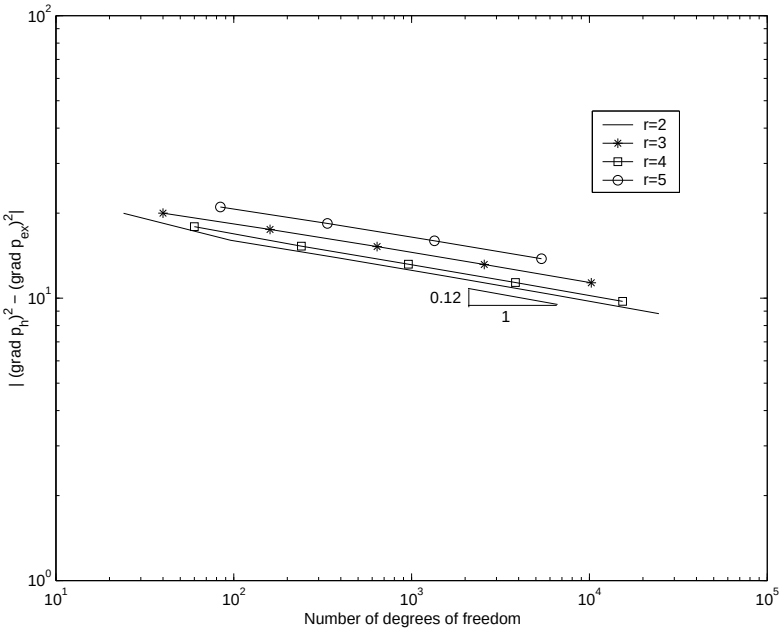

Figure 8. Discontinuous coefficients solution. Quantity A^* v. number of degrees of freedom.

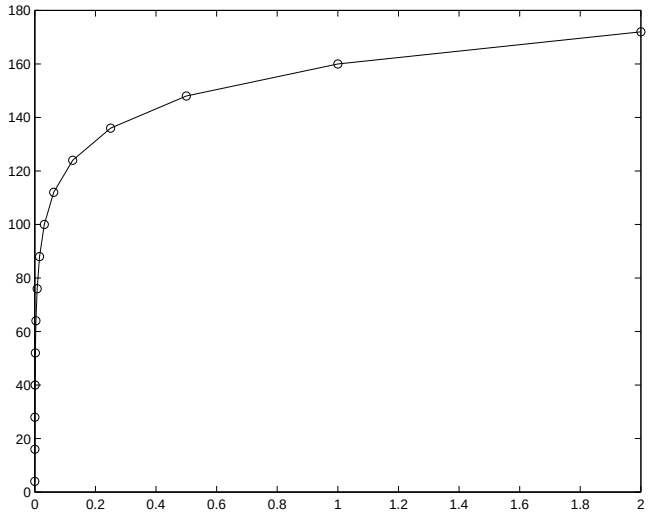

Figure 9. Discontinuous coefficients solution. Number of elements contained in a box of size H for adapted mesh.

3.3. 3D Fractured Rock

We simulate the single phase flow in a fractured porous medium. In that case, two permeable fracture zones intersect each other. A more detailed descrip-

tion can be found in [2]. The two inclined fracture zones have higher permeability than the surrounding rock, $\kappa_{\text{frac}} = 100\kappa_{\text{rock}}$. We assume no-flow boundary conditions except for the top boundary, where the pressure is imposed as

$$p(x, y, z) = y.$$

Fig. 15) shows the mesh and the quadratic approximation of the pressure. Kaaschieter [**?**] showed that the conforming finite element method yields non-physical behavior, in particular streamlines would end on the no-flow boundaries. As shown in Fig. 16, the DG approximation does not exhibit that problem. Furthermore, the residence times, i.e. the time it takes for a particle of water to reach the boundary of the domain, are comparable to those obtained in [2].

4. Conclusion

In this paper, we have shown that the flexibility of the discontinuous Galerkin method enable the use of unstructured meshes and local orders of approximation. These features can be used in single phase flow simulations, in particular in the case of heterogeneous porous media. Thanks to the local error indicator, adaptive mesh refinements can be done to achieve better accuracy.

References

[1] C.E. Baumann, An h-p adaptive discontinuous finite element method for computational fluid dynamics, Ph.D. Thesis, The University of Texas at Austin (1997).

[2] E.F. Kaasschieter, Mixed finite elements for accurate particle tracking in saturated groundwater flow, Advances in Water Resources 18 (5) (1998) 227–294.

[3] J.T. Oden and I. Babuska and C.E. Baumann, A discontinous hp finite element method for diffusion problems, Journal of Computational Physics 146 (1998) 491–519.

[4] B. Rivière, M. F. Wheeler and V. Girault, Improved energy estimates for interior penalty, constrained and discontinuous Galerkin methods for elliptic problems. Part I, Computational Geosciences 3 (1999) 337–360.

[5] B.Rivière, Discontinuous Galerkin Finite Element Methods for Solving the Miscible Displacement Problem in Porous Media, Ph.D. Thesis, The University of Texas at Austin (2000).

[6] B. Rivière and M. F. Wheeler, A posteriori error estimates and mesh adaptation strategy for discontinuous Galerkin methods applied to diffusion problems., Technical Report, Texas Institute for Computational and Applied Mathematics 00-10 (2000).

[7] M.F. Wheeler, An elliptic collocation-finite element method with interior penalties, SIAM J. Numer. Anal. 15 (1) (1978) 152–161.

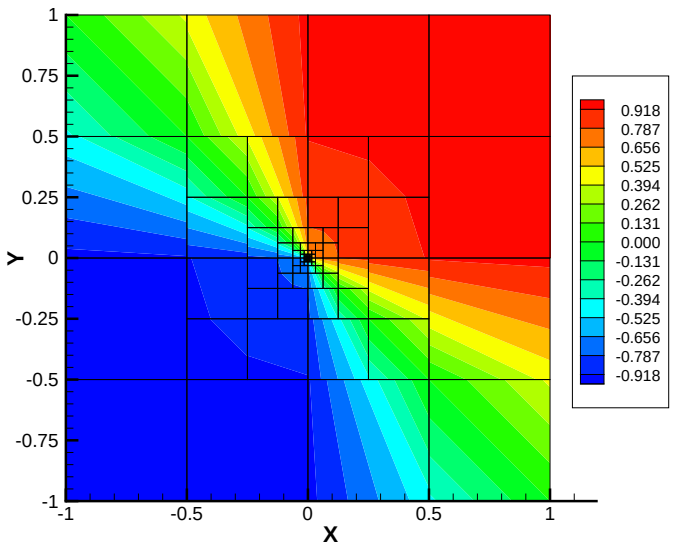

Figure 10. Discontinuous coefficients solution. Computed solution on adaptive mesh.

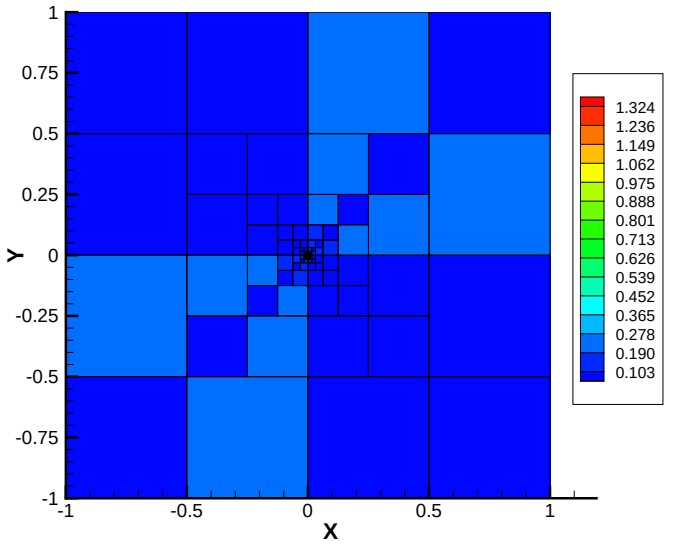

Figure 11. Discontinuous coefficients solution. Local error indicators on adaptive mesh.

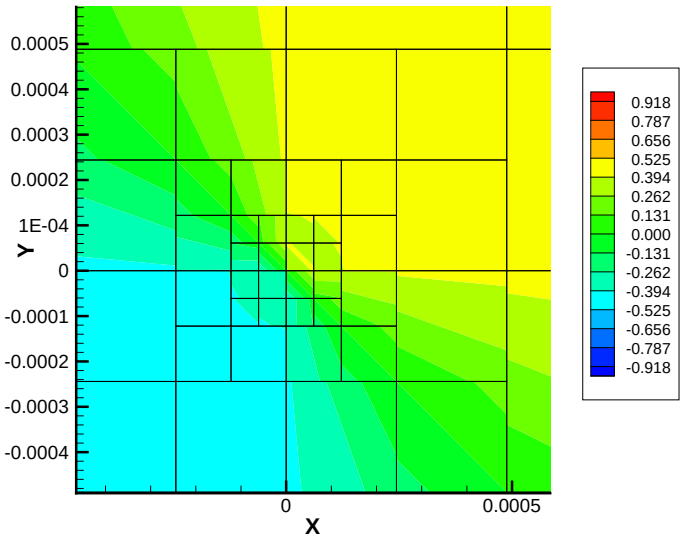

Figure 12. Discontinuous coefficients solution. Close-up view of DG solution.

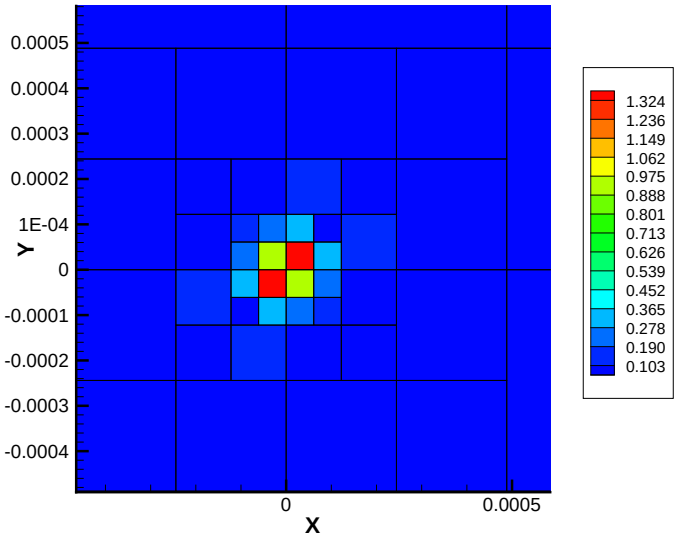

Figure 13. Discontinuous coefficients solution. Close-up view of error indicators.

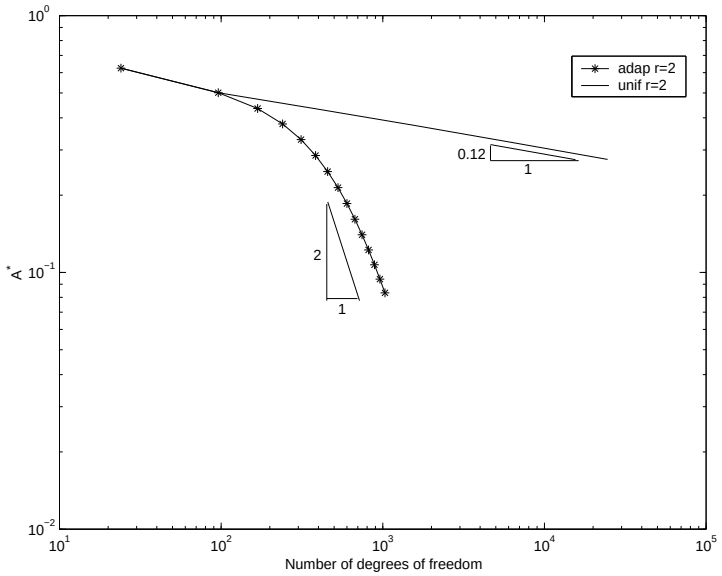

Figure 14. Discontinuous coefficients solution. Quantity A^* versus the number of degrees of freedom.

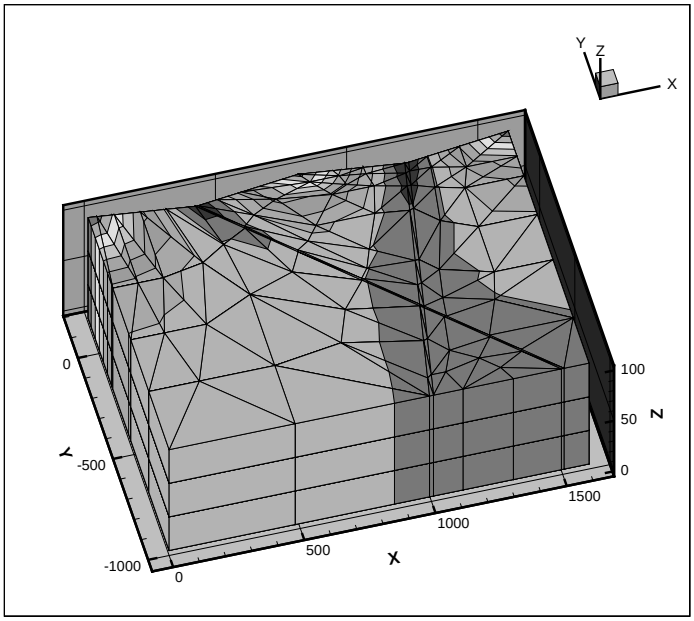

Figure 15. Fractured Rock. Pressure field.

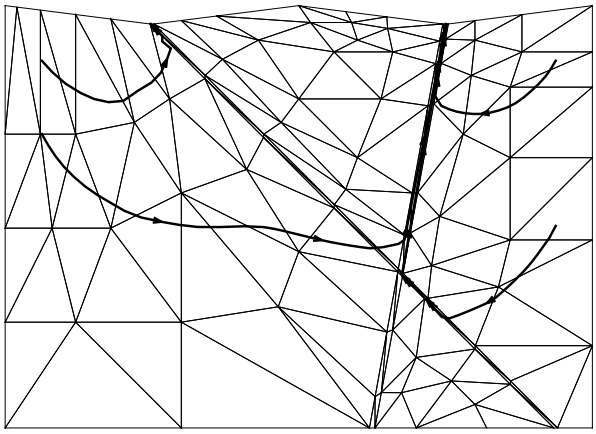

Figure 16. Fractured rock. Particle tracking.